Available online at www.sciencedirect.com
SCIENCE DIRECT®
Nuclear Instruments and Methods in Physics Research A 515 (2003) 524–542
NUCLEAR INSTRUMENTS & METHODS IN PHYSICS RESEARCH Section A
www.elsevier.com/locate/nima

Commissioning of the DAΦNE beam test facility

G. Mazzitelli, A. Ghigo, F. Sannibale, P. Valente*, G. Vignola

Laboratori Nazionali di Frascati dell'INFN, INFN, Sezione di Frascati, Via Enrico Fermi 40 Casella Postale 13, Frascati, Rome 00044, Italy

Abstract

The DAΦNE Beam Test Facility (BTF) is a beam transfer line optimized for the production of electron or positron bunches, in a wide range of multiplicities and down to single-electron mode, in the energy range between 50 and 800 MeV. The typical pulse duration is 10 ns and the maximum repetition rate is 50 Hz. The facility design has been optimized for detector calibration purposes. The BTF has been successfully commissioned in February 2002 and started operation in the same year in November. The schemes of operation, the commissioning results, as well as the first users' experience are reported here.

PACS: 41.75.Fr; 41.85.Ew; 29.40.Vj

Keywords: Electron and positron beam; Beam intensity; Calorimeters

1. Introduction

The Beam Test Facility (BTF)[1] is part of the DAΦNE ϕ-factory complex [1], Fig. 1, which includes a high current electron and positron LINAC, a 510 MeV e^- and e^+ accumulator and two 510 MeV storage rings. About 150 m of transferlines connect the different accelerators.

The e^+/e^- beam from the LINAC is stacked and damped in the accumulator ring for being subsequently extracted and injected into the Main Rings. When the injector system is not delivering beams to the accumulator, the LINAC beam can be trasported into the beam test area by a dedicated transferline (BTF line).

The BTF facility has been designed [2] to provide a defined number of particles in a wide range of multiplicities and energies, mainly for detector calibration purposes. After a brief description of the transferline layout, this paper sequentially describes the scheme for single particle production, the energy selection system and its resolution, the detectors used for the beam diagnostics, and some measurements of beam characteristics during the commissioning phase. In the last part, a "parasitic" and a "dedicated" use of the BTF is briefly discussed together with the operational experience during the first users dedicated shifts.

2. BTF description

Fig. 2 shows the BTF transferline. It is composed by a portion shared with the LINAC

*Corresponding author. Tel.: +39-06-9403-2761; fax: +39-06-9403-2427.
E-mail address: paolo.valente@lnf.infn.it (P. Valente).
[1] http://www.lnf.infn.it/acceleratori/btf/

0168-9002/$ - see front matter © 2003 Elsevier B.V. All rights reserved.
doi:10.1016/j.nima.2003.07.017

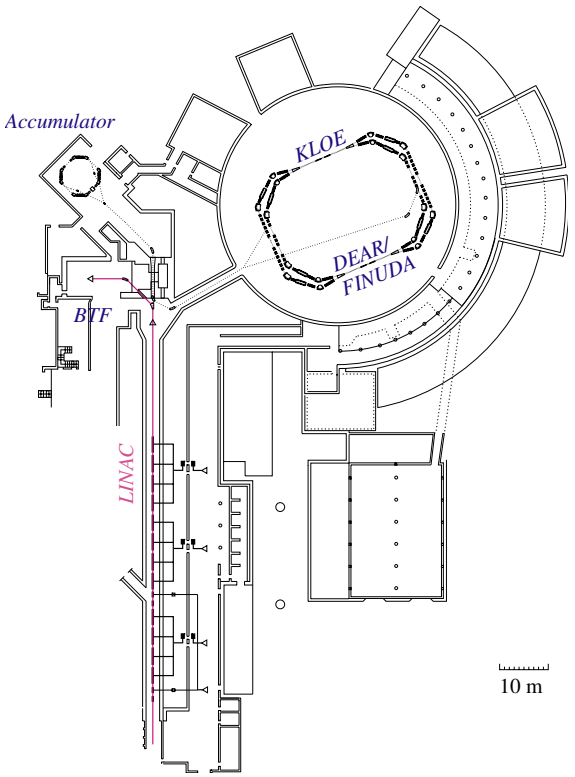

Fig. 1. Layout of the DAΦNE complex showing the LINAC, the Accumulator, the Main Rings and the Beam Test Facility (BTF).

to Accumulator transferline and by an independent part that allows transporting the beam inside the BTF experimental hall. The elements of the DAΦNE injector system and of the BTF line relevant for the BTF operation are:

- *The DAΦNE LINAC*: This 2.856 GHz linear accelerator delivers bunches of electrons with energy and current per bunch up to 800 MeV and 500 mA, respectively, or bunches of positrons with energy up to 550 MeV and current per bunch up to 100 mA. The macrobunch duration is $\sim$10 ns FWHM with a maximum repetition rate of 50 Hz. The main LINAC parameters are summarized in Table 1.
- *The LINAC to Accumulator transferline*: Downstream the LINAC, it transports the LINAC beams to the Accumulator ring. A 45° bending magnet (*Dipole* 1 in Fig. 2) allows to alternatively send the beam to the BTF area.
- *The spectrometer line*: At the beginning of the LINAC to Accumulator transferline a pulsed 6° dipole magnet deviates some of the LINAC bunches (typically 1 per second) into a separate line, where the beam energy and energy spread are measured by a spectrometer. The system is essentially composed of a 60° bending magnet with a 24-channel secondary emission monitor (hodoscope) located at its focus plane. The spectrometer resolution is $\approx$0.2% [5].
- *The energy degrader*: The insertion of this tungsten target downstream the spectrometer line allows to drammatically increase the beam energy spread for the BTF purposes, as it will be explained in Section 3.2. A linear actuator allows removing the target from the beam path and the selection of three different target thicknesses.
- *The energy selector*: The 45° bending magnet downstream the energy degrader (*Dipole* 1 in Fig. 2) has the double task of deviating the beam to the BTF hall and, jointly with the downstream collimator (*Collimator* 2 in Fig. 2), of selecting the particles by their energy.
- *The final bending magnet*: About 12 m of transferline after the energy selector, bring the beam inside the BTF experimental hall where the experimental setups are installed. At the end of the transferline a second bending magnet (*Dipole* 2 in Fig. 2) allows switching between two separate output ports 45° far each other.

All magnetic elements (dipoles, correctors and quadrupoles), as well as the slits and the degrader target, are remotely controlled and fully integrated in the DAΦNE control system [3,4].

The experimental area (former "Pion Test Facility" during the ADONE operation) that covers an area of about 100 m^2 area has two independent entrance doors, a 6 m high ceiling, several movable concrete blocks for shielding and a crane with 20 ton capability.

Fig. 3 shows the layout of the BTF experimental hall with the two transferline outputs and the position of the shielding concrete blocks, while the picture in Fig. 4 shows part of the BTF transferline inside the LINAC tunnel. Nearby to the experimental area the BTF control room allows to run

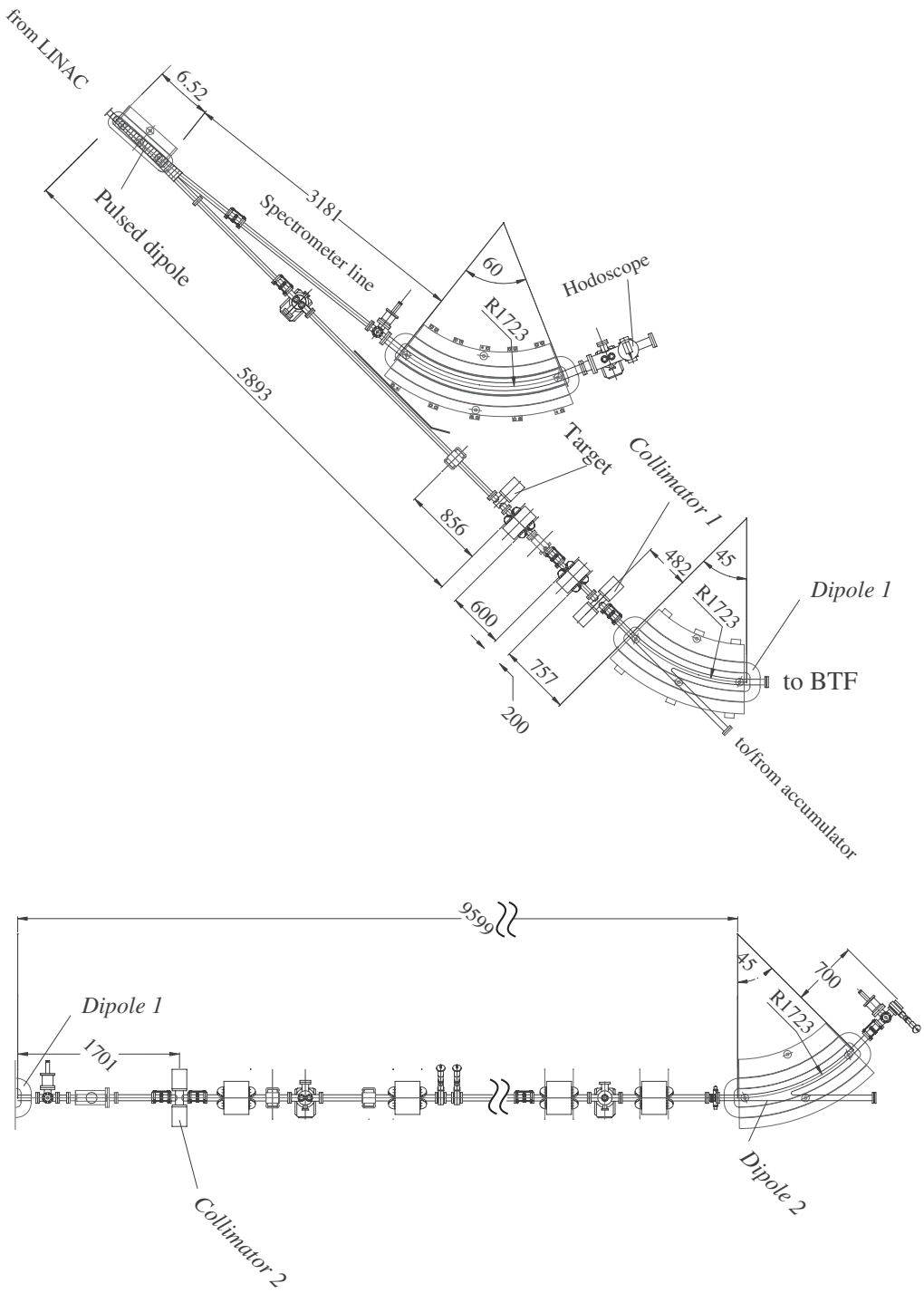

Fig. 2. The BTF transferline. Top: the first part of the line from the LINAC to the energy selector magnet (*Dipole* 1) is shown with its main elements: the pulsed magnet sending one pulse out of 50 (25) into the LINAC spectrometer system (dipole and hodoscope), the energy degrader target and the *Collimator* 1 before the energy selector magnet. Bottom: the transferline to the BTF hall where two beam output ports can be selected by *Dipole* 2.

Table 1
DAΦNE LINAC main parameters

Parameter	Value
Energy range	50–800 MeV (e^-)
	50–550 MeV (e^+)
Transverse emittance at 510 MeV (both planes)	1 mm mrad (e^-)
	10 mm mrad (e^+)
Energy spread at 510 MeV (rms)	1% (e^-)
	2% (e^+)
Repetition rate	10–50 Hz
Macro bunch duration (FWHM)	10 ns
Micro bunch duration (FWHM)	$\sim$14 ps
Maximum current	500 mA/bunch (e^-)
	100 mA/bunch (e^+)

the facility and the users set-ups conveniently. A number of different cables pulled between the experimental hall and the control room permits to bring raw signals inside the control room.

The controls for all the facility components are distributed in several racks along the line. A dedicated VME crate is demanded to the control of the different detectors used for the BTF diagnostics (see Sections 4.1 and 4.4). The facility also provides the user with several different equipments including scintillator pallets, HV crates, a VME crate with CAMAC branch, a VME controller CPU and a complete gas system for the operation of gas detectors. Four independent stainless-steel lines with four pressure-reduced heads allow using different types of gasses including carbon dioxide, isobutane, ethane, argon and other noble gases.

Finally, a remotely controlled motorized trolley (2×1 m^2 area) is available for moving detectors.

3. Main parameters and operation mode

The minimum LINAC beam current per bunch that can be reasonably measured by the LINAC and transferline current monitors is $I \approx 1$ mA. As the typical bunch duration is 10 ns, the number of particles per bunch is given by

$$N = \frac{It}{e} = 6.24 \times 10^7.$$

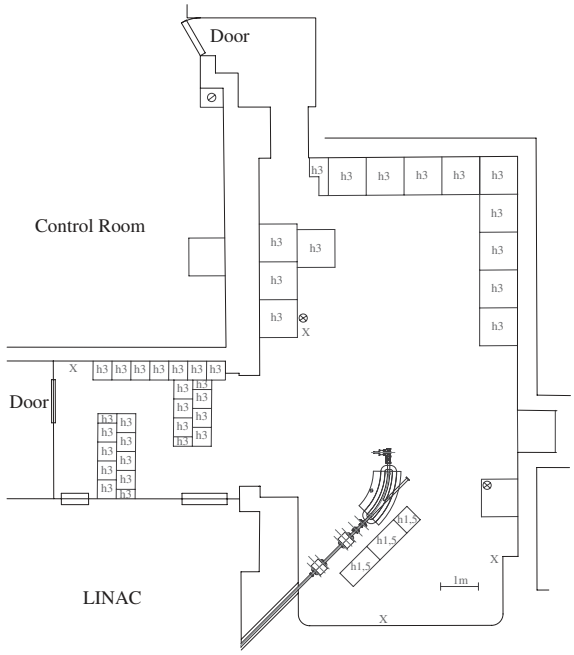

Fig. 3. Layout of the BTF experimental hall, showing the final part of the transferline with the second bending magnet (*Dipole* 2). The concrete blocks of the shieldings are also shown.

Fig. 4. The BTF transferline inside the LINAC tunnel. On the right, from the foreground: the bending magnet of the energy selector (*Dipole* 1), followed by the small vertical tower of a fluorescent screen, by the two horizontal parts of the *Collimator* 1 and by a quadrupole magnet. On the right, in the background, the transferline from the Accumulator to the Main Rings.

To reach the few particles per bunch range at the BTF, it is thus necessary to strongly reduce the number of primary e^- (e^+) coming from the LINAC.

The reduction of the particle multiplicity can be achieved with different methods. In the BTF, the

LINAC beam is first intercepted by a metallic target that highly increases the energy spread of the primary beam, then the particles are selected by energy in the energy sector. This system, which is essentially a bending-slit spectrometer, accepts only a very small fraction of the resulting energy distribution reducing the number of particles per bunch by a large and tunable factor.

The energy degrader target (see Fig. 2) is in tungsten and can present to the beam three different selectable thicknesses corresponding to 1.7, 2.0 and 2.3 radiation lengths. A fourth position allows the complete removal of the target from the beam path during the DAΦNE injection.

3.1. Energy selection resolution

In order to evaluate the energy acceptance of the selector, the geometry of the system has to be taken into account. The definitions for the relevant parameters, such as the slit apertures and distances are shown in Fig. 5.

The dispersion introduced by the bending magnet creates a correlation between the particle energy and its angular deflection in the magnet. In this situation, the relative energy spread $\Delta E/E$ becomes proportional to the relative angular dispersion $\Delta\alpha/\alpha$. The drift L_2 that follows the magnet, transforms the energy-angle into an energy-horizontal position correlation, and finally the second slit placed at the bending magnet focus allows the passage only of the particles with energy within the acceptance range set by the system. The energy acceptance of such a system can be analytically calculated obtaining [2]

$$\left|\frac{\Delta E}{E}\right| = \frac{h}{2\rho} + \sqrt{2}|x_0'|_{\max} \tag{1}$$

where the quantities in the equation are defined in Fig. 5 and $|x_0'|_{\max}$ is the maximum divergence that the particle can assume at the dipole entrance. $|x_0'|_{\max}$ can be calculated as

$$|x_0'|_{\max} = \frac{R_x + H/2}{L_1} \tag{2}$$

where H and L_1 are again defined in Fig. 5 and R_x is the maximum radius that the beam spot can assume at the output face of the target. Combining

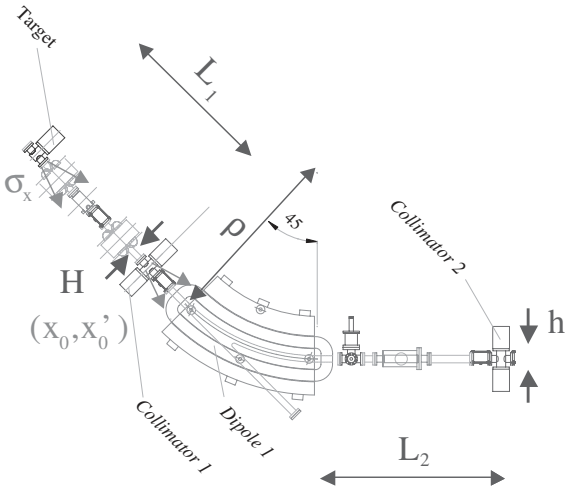

Fig. 5. Definition of the quantities relevant for the energy selector resolution: radius of curvature of the dipole, slit apertures and distances.

Eqs. (1) and (2), the total energy acceptance is given by

$$\left|\frac{\Delta E}{E}\right| = \frac{h}{2\rho} + \sqrt{2}\left(\frac{R_x}{L_1} + \frac{H}{2L_1}\right). \tag{3}$$

Using in Eq. (3) for the BTF case $\rho = 1.723$ m, $L_1 = 1.4750$ m, and the typical values used in the November–December 2002 shifts: $h = 5$–10 mm, $H = 5$–10 mm and $R_x \simeq 5$ mm, a $\approx 1\%$ upper limit for the energy acceptance can be estimated. Table 2 summarizes the mechanical and positioning characteristics of the upstream and downstream slit systems.

The nominal energy of the selector system, E_{sel}, is calculated from the current setting of the *Dipole* 1 magnet using its nominal magnetic length of 1.723 m and the experimental field/current excitation curve shown in Fig. 6: the relation is linear up to 400 A, corresponding to ≈ 590 MeV (the magnetic measurements were performed by the manufacturer, ANSALDO [6]). An independent absolute calibration of the LINAC energy measurement performed by the DAΦNE spectrometer can be provided by the resonant production of the ϕ meson in the DAΦNE Main Rings with e^+e^- collisions, since the effects of the combined effects of Accumulator and Main Rings momentum acceptance is $\sim 1\%$.

Table 2
The main parameters of the energy selector (tungsten) slit system

Slit	Parameter	Value
Upstream (*Collimator* 1)	Transverse dimensions	30 mm × 60 mm
	Thickness	35 mm
	Aperture range	0.1–55 mm
	Positioning step	0.1 mm
Downstream (*Collimator* 2)	Transverse dimensions	35 mm × 70 mm
	Thickness	35 mm
	Aperture range	0.1–62 mm
	Positioning step	0.02 mm

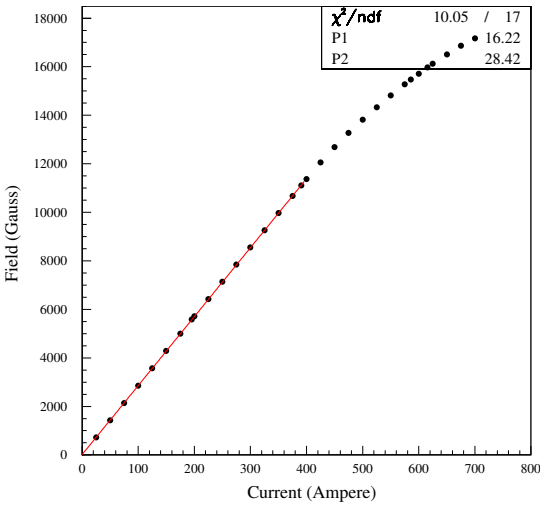

Fig. 6. Excitation curve for *Dipole* 1 magnet.

3.2. Single particle per bunch production

To operate in the single particle mode, the incoming beam has to be attenuated by a factor as large as 10^8, by means of the energy degrader and selection systems discussed above. The most effective knob that allows adjusting the number of particles per bunch is the selected energy, E_{sel}. In fact, by selecting different values for E_{sel} a different fraction of the degraded beam will be accepted.

The expected multiplicity as a function of the selected energy can be calculated by integrating the energy distribution of the target emerging particles over the accepted energy range. A simple estimate of the energy distribution out of a target of thickness $t = x/X_0$ in radiation length units can be obtained using the well-known formula, in the so-called "Rossi approximation B" [7]:

$$f(E, E_0, t) = \frac{1}{E_0} \frac{[\ln(E/E_0)]^{(t/\ln 2)-1}}{\Gamma(\frac{t}{\ln 2})} \quad (4)$$

where E_0 is the energy of the particle initiating the shower and Γ is the Euler function. The energy distribution calculated using Eq. (4) is shown in Fig. 7. This distribution, however, does not take into account the angle of the emerging particles, because not all those secondary electrons will be accepted by the collimator and transported. Moreover, the beam-line itself limits the maximum angular divergence (in the vertical plane) to 6 cm/1.475 m ≈ 4 mrad.

In order to include those effects in the estimate of the expected number of particles as a function of the selected energy, a Monte Carlo simulation, based on GEANT [8], has been developed; the simulation includes the target and the upstream collimator, as well as the beam-pipe acceptance. Fig. 8 shows the simulated electron energy distributions without angular cut and for $\theta \leqslant 4$ mrad—corresponding to the beam-pipe acceptance (open collimator)—for the three possible

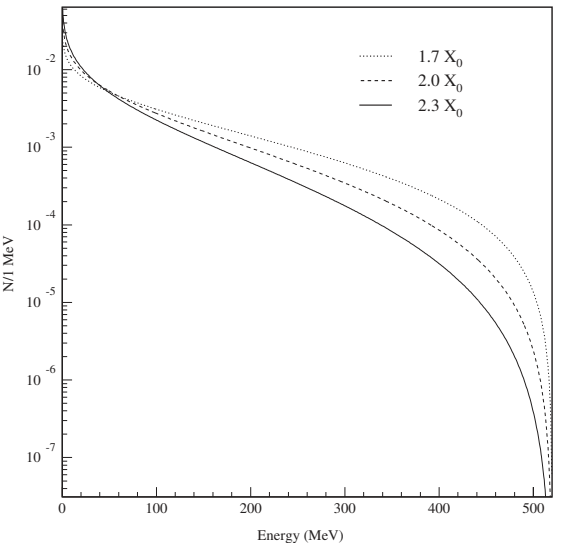

Fig. 7. Electron energy distributions out of a 1.7, 2.0, 2.3 X_0 target, calculated according to the Rossi formula of Eq. (4).

target thicknesses. A large number of Monte Carlo events have to be simulated to have a significant estimate also when E approaches E_0 and few particles survive. In the Monte Carlo distributions of Fig. 8, 10^8 primary electrons have been simulated, corresponding to a LINAC current of 1.6 mA (for a 10 ns bunch length).

The number of accepted electrons as a function of E_{sel} is then simply calculated by integrating the energy distribution, with the proper angular cut for the chosen collimator aperture, around each E_{sel}. The integration range width should be chosen according to the energy resolution corresponding to each given collimator aperture. However, as shown before, a 1% resolution is a good approximation for a wide range of slit apertures, and by integrating the distribution of Fig. 8(b) over 1% slices the expected number of electrons as a function of E_{sel} can be finally obtained. Fig. 9 shows the case for a target thickness of $1.7X_0$.

The number of particles estimated from the Monte Carlo simulation has to be considered as an upper limit, since it does not take into account the downstream transport efficiency. A detailed calculation of the transferline efficiency would require to combine single-particle simulation codes (essentially based on GEANT [8]) with the beam transport calculation codes (such as MAD [9]), and is currently under study.

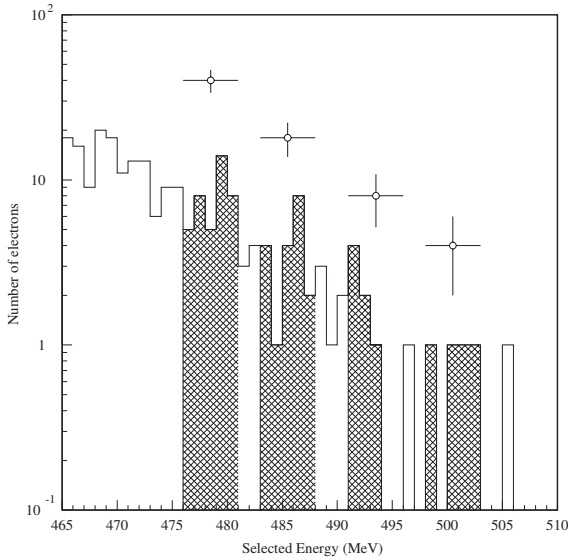

Fig. 9. Integrating the energy distribution of electrons emerging from the target (for $1.7X_0$ depth) over 1% slices (shaded area), the expected number of particles as a function of the selected energy (open points) can be estimated from the Monte Carlo.

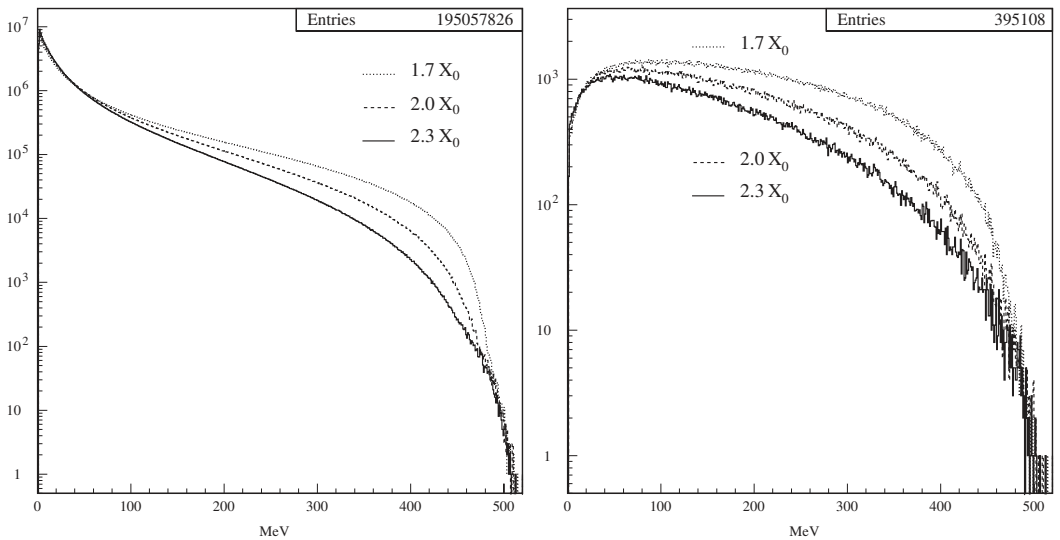

Fig. 8. Electron energy distributions: (a) without angular cut and (b) for $\theta \leqslant 4$ mrad, for the three different degrader target thicknesses, at the exit of the first slit collimator (*Collimator* 1). Monte Carlo simulation with 10^8 primary electrons.

4. Commissioning results

The BTF commissioning started in February, 2002. The electron beam was transported in the BTF transferline using the two high-fluorescence targets downstream each of the BTF bending magnets (see Fig. 2). The very first beam was injected into the BTF line on February 4, 2002 and dumped onto a lead Faraday cup. Fig. 10 shows the transverse beam profile on the flag inside the BTF hall.

For the correct operation of the energy selector, it is very important that the beam is centered in the selector magnet vacuum chamber. This was achieved by monitoring the (non-attenuated) beam with both the fluorescent flags and the LINAC beam position monitors and by closing the collimators upstream and downstream the bending magnet in a symmetric way.

For radiation safety reasons, from then on no beam was allowed into the BTF hall without inserting the attenuating target. In single particle mode, and also in the intermediate range with up to many thousands of particles per bunch, no conventional beam diagnostics is sensitive enough to be used and the beam must be monitored by means of particle detectors.

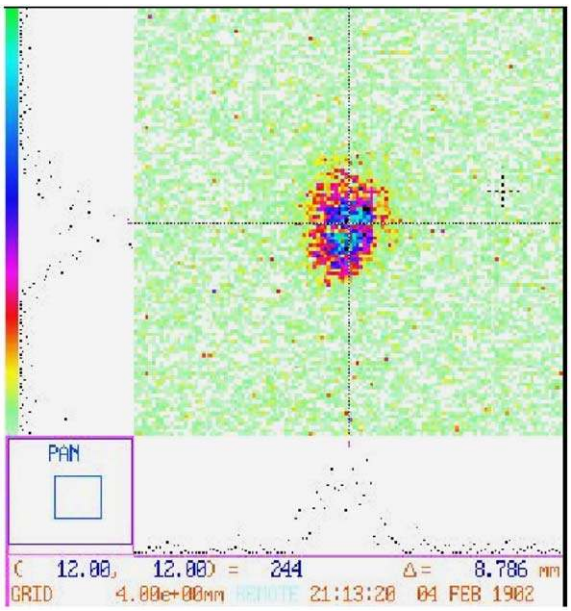

Fig. 10. High-fluorescence target image of the first beam injected into the BTF hall, on February 4, 2002.

4.1. Diagnostic detectors: calorimeters

Two different calorimeters positioned at the two BTF output ports have been used as main diagnostic devices.

Both detectors are lead/scintillating fiber calorimeters of the KLOE type [10], with single side photomultiplier readout. They are both composed by a stack of 0.5 mm thick grooved lead foils, alternating with an equal number of layers of 1 mm scintillating fibers (blue-green, type Po.Hi.Tech-0046), with 1.35 mm pitch, giving a 5 g/cm^3 density composite. The two calorimeters have different readout segmentation:

Calorimeter 1: It is a cut-out of the KLOE barrel calorimeter *Prototype 0* and is composed by $\approx$200 lead/scintillating fiber layers of 13.2×40 cm^2 for a total thickness of 24 cm, corresponding to $\approx 15X_0$. It is segmented in 4.4×4.4 cm^2 square cells with one-side only readout. For each cell, the light is collected by a glued guide, consisting of a tapered mixing part with quadrangular entrance and circular exit terminating with a Winston cone, coupled to a Hamamatsu R1398 photomultiplier. A schematic view of the lead/fibers arrangement and of the segmentation of Calorimeter 1 is shown in Fig. 11; further details on this calorimeter can be found in Ref. [11].

Calorimeter 2: It is one of the small calorimeters used for the online measurement of the DAΦNE luminosity [12]. It has the same lead/fibers composition of Calorimeter 1, but has smaller transverse dimensions, 12.2×12.2 cm^2, and thickness, 18.4 cm, corresponding to $\approx 11.5X_0$. It is equipped with two plastic guides concentrating the light onto a single 3″ cathode photomultiplier (Hamamatsu H6155-01), as schematically shown in Fig. 11.

The performances of this kind of calorimeters have been extensively studied [10,11] and the main features are a sampling fraction of $\approx$15%, a good energy resolution and an excellent timing

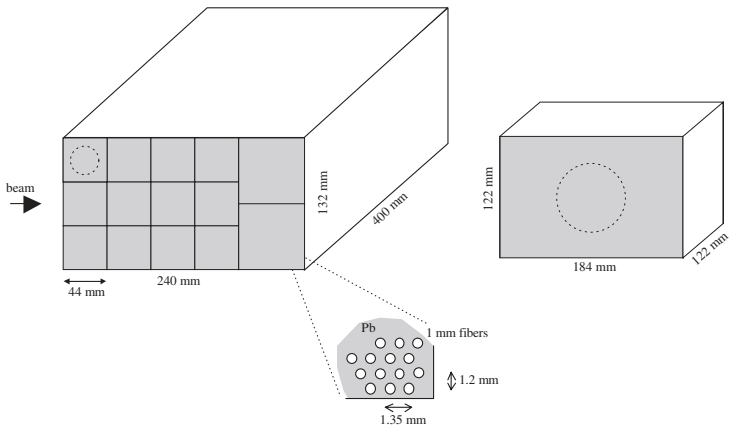

Fig. 11. Schematic view of the calorimeters: "Calorimeter 1", the 14-cells KLOE calorimeter Prototype 0 (left); "Calorimeter 2" the single-PMT DAΦNE luminometer (right).

resolution:

$$\sigma_E/E = 4.7\%/\sqrt{E(\mathrm{GeV})},$$

$$\sigma_t/t = 54\ \mathrm{ps}/\sqrt{E(\mathrm{GeV})}.$$

The $14+1$ analog signals from the calorimeters are suitably delayed ($\approx$200 ns) and fed to a VME charge ADC (CAEN V792), with a resolution of 0.25 pC/count, integrating over a gate of 250 ns width. The gate signal is generated starting from a digital reference signal from the LINAC gun timing circuit (properly re-formed and timed). The analog signals are also digitized by means a VME low-threshold discriminator (CAEN V814) with a threshold of 35 m/50 Ω. The time of each channel is measured by means of a VME TDC (CAEN V775), in common stop mode (again given by the reference signal from the LINAC gun), with a resolution of 35 ps/count.

The VME controller is a VMIC 7740 Pentium III CPU with a Tundra VME-PCI bridge chip, running Red Hat Linux 7.2. The operating system is down-loaded over a private Fast-Ethernet network from a dedicated server (also running Red Hat Linux 7.2) that provides the remote filesystems for the data storage.

All the DAQ programs have been developed using the LabVIEW 6.0 environment with the following scheme: a low-level task continuously runs on the VME controller CPU waiting for a new event and when this happens it reads the VME bus and stores all the read-out data in a temporary buffer of defined length (usually 100 events at 25 Hz repetition rate). A dedicated high-level application accesses the data in the buffer and allows storing the data into an output file. This scheme permits online monitoring using histograms or time-charts. The relevant informations on the run conditions (date, number of events, magnet settings, slit settings, repetition rate, etc.) are also automatically stored into a relation database on a dedicated MySQL server, and are accessible as an "electronic logbook" from the BTF Web site.

4.2. Single electron measurement

During the major part of the BTF data taking, the LINAC was optimized for performing studies in the single particle mode with electron beams of 510 MeV energy and 4–5 mA current per bunch. The LINAC repetition rate of 25 Hz[2] and the bunch length of $\approx$10 ns were the same used for the normal accumulator injection. The typical (total) aperture for both the upstream and downstream slits was 2 mm. With this configuration only few electrons reached the diagnostic detectors.

Due to the good energy resolution of the calorimeters, $\approx$7% at 500 MeV, the number of

[2] Actually, only 24 pulses were sent to the BTF line since the first pulse was always deviated into the spectrometer line for the measurement of the beam energy.

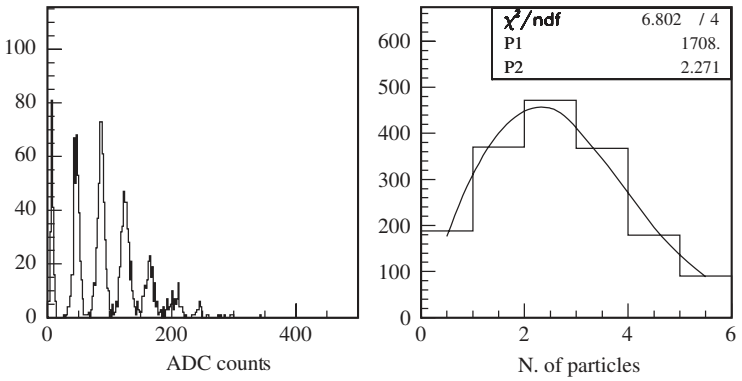

Fig. 12. Counting electrons in Calorimeter 2 ($E_{sel} = 471$ MeV, HV = 1 kV): charge spectrum (left), and Poisson fit of the average number of particles in each peak (right).

produced electrons can be counted simply by measuring the total deposited energy E. In fact, $n = E/E_1$, where E_1 is the energy deposited by a single electron. The relative experimental error on the total energy deposited by n electrons is given by:

$$\frac{\sigma_E}{E} = \frac{1}{\sqrt{n}} \frac{\sigma_{E_1}}{E_1} \tag{5}$$

where we neglected the beam energy spread much smaller than the detector resolution. With this assumption the *absolute* width of the nth Gaussian peak is given by

$$\sigma_n = \sqrt{n} \frac{\sigma_{E_1}}{E_1}. \tag{6}$$

The left plot of Fig. 12 shows an example of ADC spectrum from the Calorimeter 2 system. The pedestal was subtracted and the selected energy was $E_{sel} = 471$ MeV. The individual peaks corresponding to $0, 1, \ldots, n$ electrons per bunch can be easily identified.

The total number of events in each peak are proportional to the probability of producing n particles. If $\bar{n}$, the average number of produced particles is small, as in this case, this probability should be distributed according to the Poisson statistics:

$$P(\bar{n}; n) = \frac{\bar{n}^n}{n!} e^{-\bar{n}}.$$

The right plot of Fig. 12 shows the number of events for each peak and the Poisson function fit of the data giving an average number of particles per bunch of $\bar{n} = 2.3$.

There is an intrinsic limit in the use of this particle counting method. In fact, Eq. (6) shows that the absolute width of the peaks increases with n, so that when the average multiplicity increases the peaked structure in the energy distribution gradually disappears approaching a Gaussian shape. This technique can measure *event by event* the number of particles per bunch as long as the peaks are clearly separated, e.g. at 3σ. The minimum of the nth Gaussian overlaps with the maximum of the $(n-1)$th when

$$(n - 3\sigma_n)E_1 \simeq (n-1)E_1$$

corresponding to:

$$n \simeq \frac{1}{9(\sigma_{E_1}/E_1)^2}$$

that in our case gives a limit of $n \approx 20$.

Anyway, for larger n, the *average* multiplicity $\bar{n}$ can still be statistically estimated from the average value of the Gaussian distribution for the total deposited energy: $\bar{n} = \bar{E}/E_1$.

In this case the fluctuations of the number of particles in the bunch, $\sigma_n^2 = \bar{n}$ give the dominant contribution to the relative width of the measured energy distribution,

$$\frac{\sigma_{\bar{E}}}{\bar{E}} = \frac{\sqrt{\bar{n}}}{\bar{n}}.$$

The previous equation holds if the LINAC primary beam intensity fluctuations can be neglected. For the DAΦNE LINAC these can be roughly extimated to be $\delta_{\mathrm{LINAC}} \approx 15\%$ [2]. This approximation becomes inaccurate for high multiplicity values, where the approximately constant contribution δ_{LINAC} is no longer negligible with respect to the pure Poisson statistics term:

$$\sigma_n/n = \sqrt{1/\bar{n} + \delta^2_{\mathrm{LINAC}}}.$$

Fig. 13 shows an example of a high multiplicity spectrum of E/E_1. The single peaks corresponding to the discrete values of n are no longer resolved, but the average number of particles can still be estimated by a Gaussian fit, $\bar{n} \simeq 40$.

Another possible limitation in using this particle counting method is given by the detector saturation. Among the different factors that make the signal being no longer proportional to the number of particles we want mentioning the saturation of the ADC scale, of the photomultiplier gain and of the scintillation light yield. In our case, the photomultiplier gain saturation is the more important.

Thanks to the excellent performances of the lead/scintillating fibers calorimeter, the time distribution of the energy depositions should reflect the time structure of the LINAC pulse; in particular, an almost flat distribution, 10 ns wide, should be observed. On the other hand, the time resolution of the fibers at these energies is not good enough to resolve the ~ 14 ps of the microbunch structure. The right plot of Fig. 14 shows the time distribution for the same events of Fig. 12 together with the correlation with the measured pulse height. Even though a slewing effect is clearly visible, the width of the distribution is essentially the expected 10 ns for the first peaks, while the width gets smaller when more than one electron is detected, since the used TDC is single-hit and can only measure the time of the fastest signal.

The same results can be obtained using Calorimeter 1, once the gains of the different 14 cells are properly equalized. The calibration of each cell is performed by selecting the horizontal cosmic rays, traversing the detector. The energy deposited in the cell by a minimum ionizing particle (1 MIP) is used as reference, and the HV settings are adjusted in order to equalize all the channel responses. Fig. 15 shows an example of cosmic ray spectrum, with a Landau distribution fit.

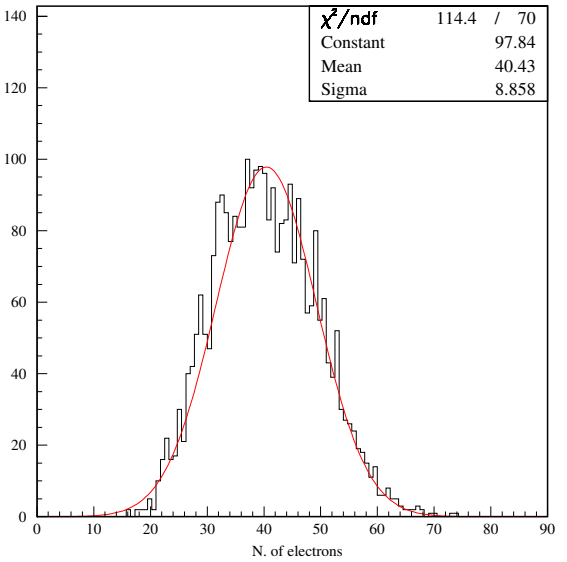

Fig. 13. The signal from Calorimeter 2 is normalized to the average deposited energy of a single electron, giving the number of particles per bunch: $n = E/E_1$.

Calorimeter 1 has been mainly used for detecting low-energy electrons. Fig. 16 shows an example of the total energy deposited in Calorimeter 1 expressed in MIP units. The channel gains were equalized and the selected energy was $E_{\mathrm{sel}} = 80$ MeV. The peaks relative to one or two electrons per bunch are still resolved and have been fitted with a sum of two Gaussians.

The measured average energy should be proportional to the incoming beam energy, while the resolution should scale as $1/\sqrt{E_{\mathrm{sel}}}$. This can be experimentally verified by performing the same energy measurement for different E_{sel} values by changing the first dipole current. Fig. 17 shows the average value and the width of the single electron peak as a function of E_{sel}. The observed energy is reasonably proportional to the beam energy, and the relative width shows a $1/\sqrt{E_{\mathrm{sel}}}$ behavior, as expected. The slight nonlinearity in the energy curve is mainly due to the fact that during the

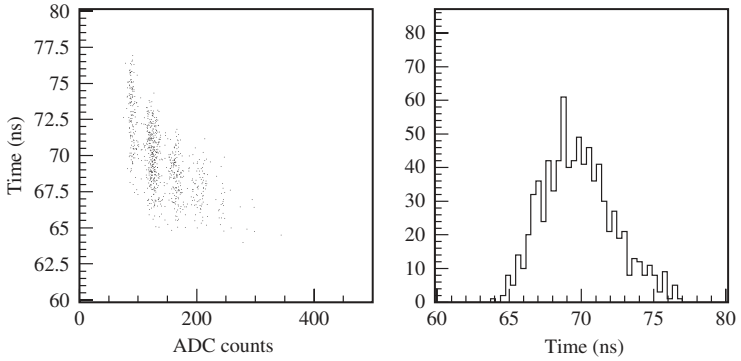

Fig. 14. Counting electrons in Calorimeter 2 ($E_{sel} = 471$ MeV, HV = 1 kV): time vs. charge distribution (left) and corresponding time spectrum (right).

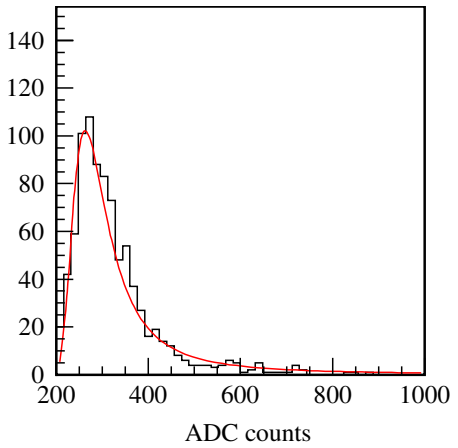

Fig. 15. Calorimeter 1: example of 1 channel cosmics spectrum with superimposed Landau fit.

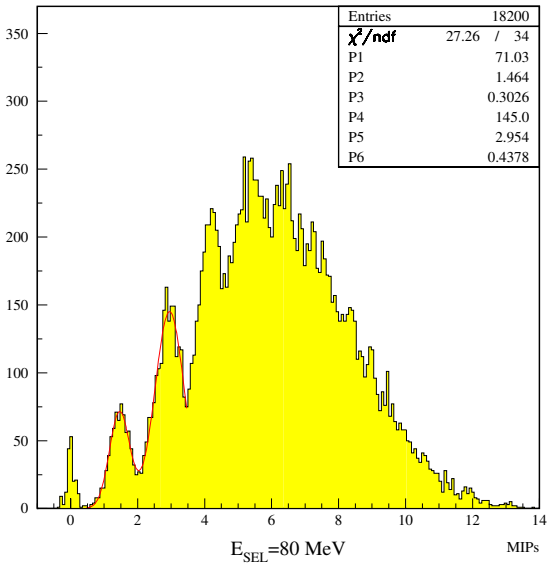

Fig. 16. Energy deposited in Calorimeter 1 for $E_{sel} = 80$ MeV after gain equalization. The Gaussian fit to the first and second electron peak is also shown.

measurement the energy selector magnet *Dipole* 1 was not systematically cycled.[3]

Even if no high sensitivity beam profile monitor was available during the 2002 shifts, an estimate of the beam spot size was obtained by measuring the particle multiplicity as a function of the collimator aperture. Fig. 18 shows the measured average multiplicity as a function of the aperture in *Collimator* 2 (downstream the bending magnet). The saturation value is consistent with what expected for a beam of a few mm size.

4.3. High multiplicity measurement

As discussed in Section 3.1, the most effective way to change the average number of particles per bunch is by changing the selected energy. In particular, for *constant* LINAC energy and intensity and for a *given* setting of the collimators,

[3] In order to control the hysterisis effects, a power cycling of the magnet is required. The magnet is sequentially brought to saturation at the maximum current, set back to zero current and finally brought to the operation current.

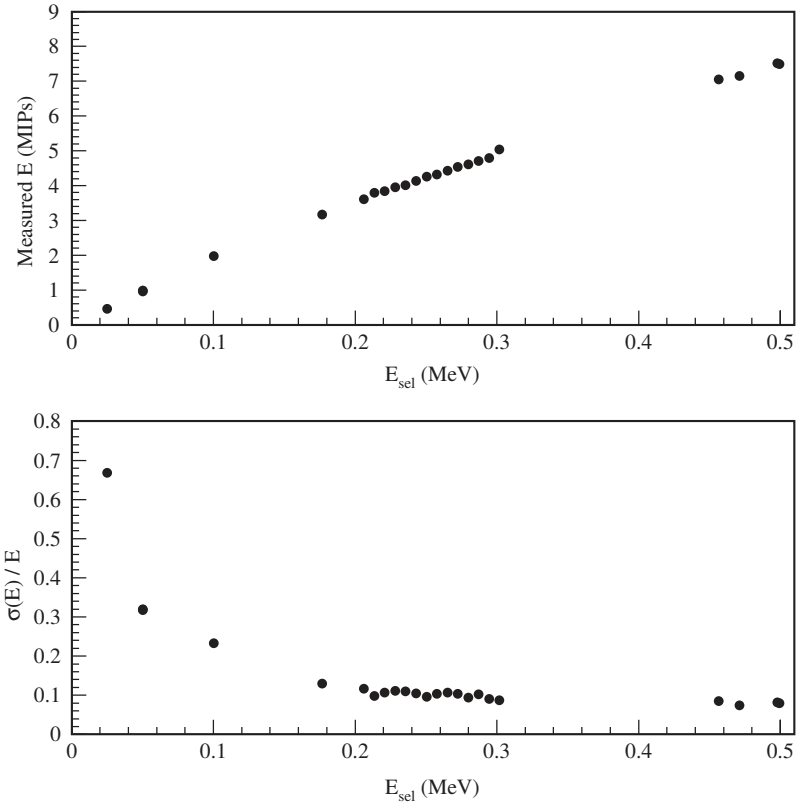

Fig. 17. Energy deposited in Calorimeter 1: the average (top) and relative width (bottom) of the Gaussian fit to the first electron peak is shown as a function of E_{sel} (calculated on the basis of the bending magnet setting).

the multiplicity increases by lowering the chosen E_{sel}.

In order to span a wider multiplicity range, Calorimeter 2 has been generally operated at a lower gain than the optimal one for the energy resolution (as in Calorimeter 1 case). In this configuration, the response of the detector is still proportional to the number of electrons up to ≈ 10 particles. Fig. 19 shows the average value of the peaks in the ADC spectrum after the pedestal subtraction and the linear fit to the data. The excellent linearity indicates essentially no saturation.

Keeping all the parameters constant and lowering the selected energy more and more, the multiplicity can be progressively increased. In the limit in which the number of particles can still be measured with a reasonable resolution (as discussed in Section 4.2), the number of produced

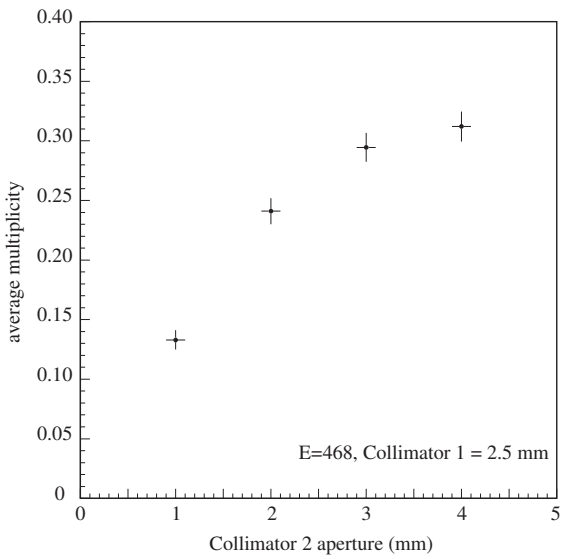

Fig. 18. Measured multiplicity as a function of *Collimator* 2 aperture.

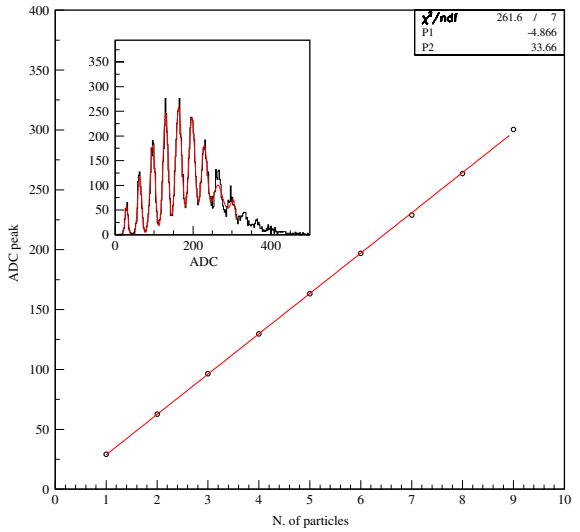

Fig. 19. Counting electrons in Calorimeter 2 ($E_{sel} = 442$ MeV, HV = 1 kV): peaks linearity. Inset: a multi-Gaussian fit to the ADC spectrum.

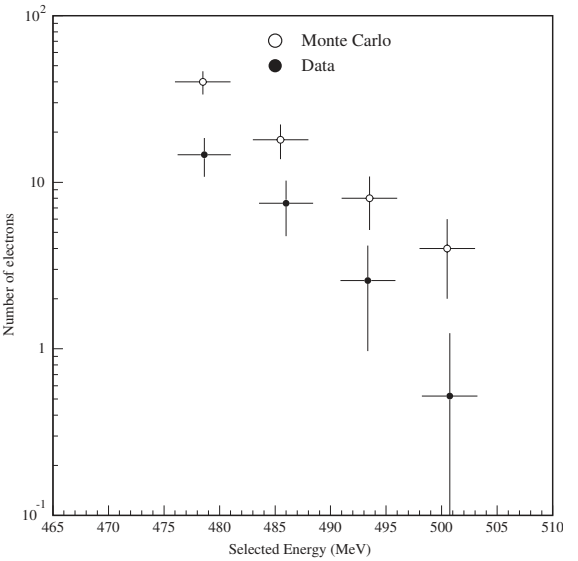

Fig. 20. Expected number of particles per bunch as a function of the selected energy. The Monte Carlo calculation (empty dots) is compared with the experimental data (full dots). The target thickness was $1.7X_0$ and the energy acceptance was 1%.

particles per bunch as a function of the selected energy can be compared with what expected from the Monte Carlo simulation described in Section 3.2. Fig. 20 shows the comparison between the Monte Carlo and the experimental distributions for the average number of particles $\bar{n}$ as a function of E_{sel}. The shapes are pretty similar but the measured values are systematically smaller than the simulated ones. Such a difference can be reasonably attributed to losses in the BTF transferline downstream the energy selector.

An alternative way of tuning the multiplicity is obtained by changing the aperture of the upstream and/or downstream slits. In such a scheme, the resolution of the energy selector is affected as well, but, as discussed in Section 3.2 by a relatively small amount in any case much smaller than the resolution of our calorimeters. The measured multiplicity will increase by opening the slits until the beam spot size (*at the downstream slit*) is exceeded (as discussed in Section 4.2).

4.4. Diagnostic detectors: Cherenkov counter

Going further up in the number of particles per bunch the calorimeters are no longer usable due to saturation effects (see Section 4.2). In order to overcome this difficulty a new diagnostic device was developed. The new detector, conceived and tested collaboration with the AIRFLY group [13], was optimized for multiplicities in the $\bar{n} = 100$–1000 range (and higher).

The system is essentially a counter using the Cherenkov light emitted by the relativistic particles[4] traversing a PLEXIGLAS radiator. The radiator that has a circular section is shaped as a bent cylinder (2 cm diameter) for separating the beam from the Cherenkov light by total internal reflection. A conical shape allows matching the radiator with a photomultiplier tube (PMT). No optical connection exists between the radiator and the PMT giving the possibility of interposing a calibrated optical filter (fused silica neutral density filters) between the radiator and the PMT. In this way, it is possible to attenuate the Cherenkov light extending the dynamical range of the counter.

[4] In the BTF the energy ranges from 50 to 800 MeV making the particles always relativistic.

The analog signal from the photomultiplier is properly delayed and sent to the same DAQ chain used for the two calorimeters where it is integrated using the same 250 ns gate signal (see Section 4.1). The discriminator threshold is decreased to 8 mV/50 Ω, in order to be sensitive to the signal generated by the passage of a single electron.

The Cherenkov light yield, and in turn the phototube analog signal, are proportional to the number of electrons traversing the radiator up to a very high number of electrons. Fig. 21 shows, for the few particles range, the comparison between the charge spectrum from the Cherenkov detector and the energy spectrum from the calorimeter. Because of the very small signal and of the limited resolution, the Cherenkov counter is not able to resolve the peaks relative to one or to few electrons per bunch. The estimated beam spot size at the detector position ($\sigma \approx 5$ mm, see this subsection continuation and Section 4.2) is comparable with the diameter of the radiator (20 mm) spoiling the detector resolution specially in the single electron case (see Fig. 21).

Fig. 22 shows the same comparison between the two detectors now in the high multiplicity regime. The same data of Fig. 13 were used where the average number of electrons per bunch was ≈ 40 and the selected energy was $E_{\mathrm{sel}} = 471$ MeV. A strong correlation between the two signals is clearly visible. The ratio between the two signals, which allows the cross-calibration between the two detectors, has been estimated as the average value of the distribution of the ratios for each individual measured point.

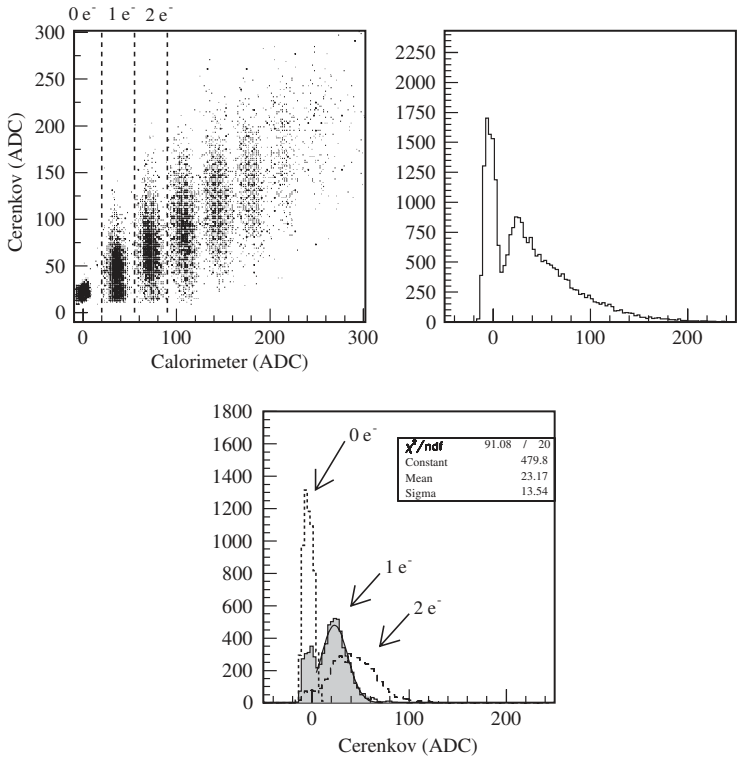

Fig. 21. Top left: scattered plot of the signal from the Cherenkov counter vs. the signal from the calorimeter (in ADC counts units). Top right: the raw spectrum of the Cherenkov signal. Bottom: three different spectra obtained from the same data but requiring 0,1,2 electrons in the calorimeter (the relative cuts are shown by the dashed lines in the top left of the scatter plot). When no electrons are detected in the calorimeter only pedestal is measured at the Cherenkov (dotted line histogram). When a single electron is detected in the calorimeter, the peak relative to one electron is clearly visible also in the Cherenkov (shaded histogram) even if the part of the signal overlapping with the no electrons position reveals some inefficiency in the detector due mainly to its small acceptance, the broader peak in the Cherenkov spectrum (dashed line histogram) corresponds to two electrons in the calorimeter.

The same measurement has been repeated for the same conditions but interposing a calibrated optical filter—with attenuation factor 10—between the radiator and the photomultiplier. Fig. 23 shows the results of the measurement with this new configuration. The measured attenuation factor was 10.4 ± 0.3. The described measurements allowed to calibrate the Cherenkov counter that was then used for performing measurements with beam multiplicity up to ≈ 1000 particles, as shown in Fig. 24.

The Cherenkov counter and calorimeter signals have also been used for measuring the horizontal acceptance of the beam line. As described in Section 2, the last dipole magnet, *Dipole* 2, allows to select between the straight and the 45° angle exits. If the bending angle of the dipole is modified by changing the excitation current of the magnet, the observed yield in the detectors should remain constant until the beam goes out of the horizontal angular acceptance of the detector or hits the vacuum chamber.

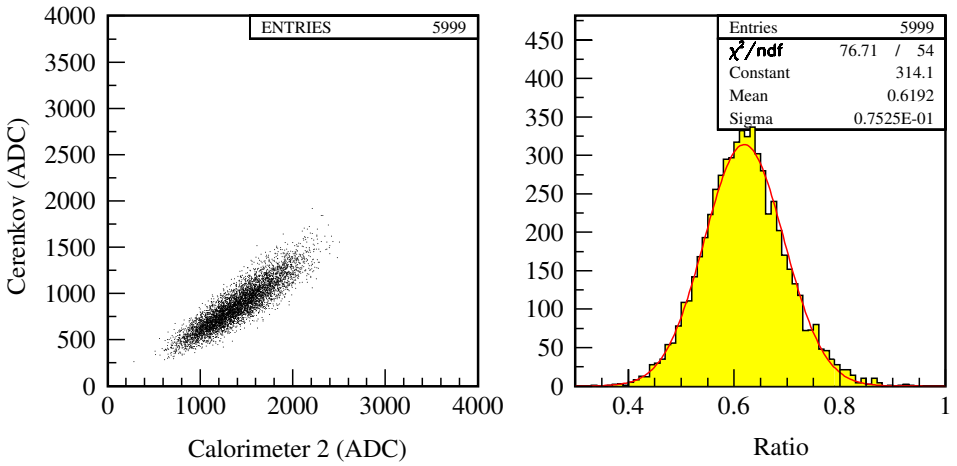

Fig. 22. Left: signal in the Cherenkov counter vs. signal in the calorimeter, in ADC counts. Right: distribution of the ratio between the two signals with the Gaussian fit used for the estimate of the average ratio. $E_{sel} = 471$ MeV case.

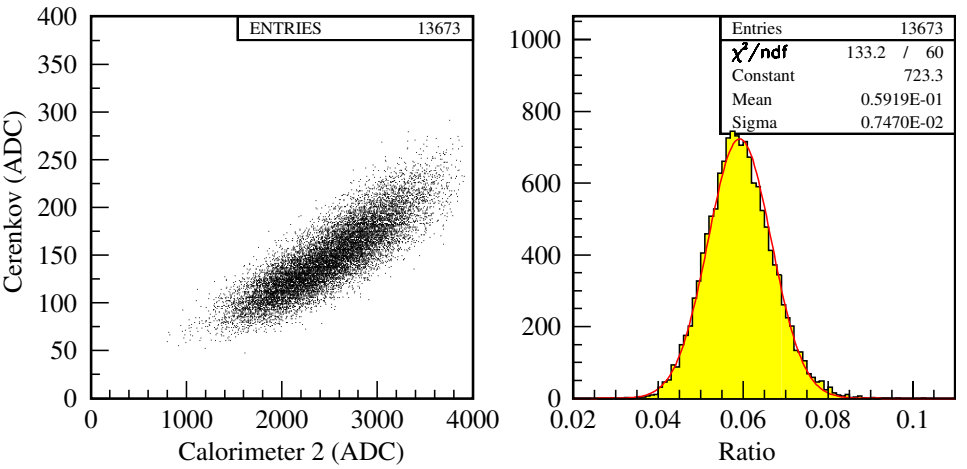

Fig. 23. Left: signal in the Cherenkov counter vs. signal in the calorimeter, in ADC counts. Right: distribution of the ratio between the two signals with Gaussian fit when an optical filter with attenuation factor = 10 is inserted between the radiator and the photomultiplier ($E_{sel} = 471$ MeV). For these measurements, the beam intensity was increased by opening the downstream collimator for increasing the signal in the Cherenkov counter.

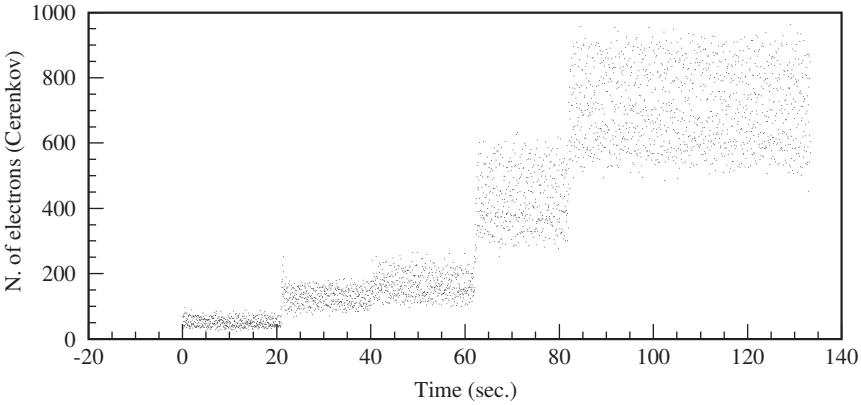

Fig. 24. Measurement of number of particles per bunch by using the Cherenkov counter (after calibration with Calorimeter 2) as a function of time. The multiplicity during the run was increased by opening the collimators.

The described situation was clearly observed in the measurement shown in Fig. 25. The measured multiplicity in Calorimeter 2 and in the Cherenkov counter is shown as a function of the bending angle. While the yield in the Cherenkov reflects the shape of the PLEXIGLAS radiator and drops to zero when the beam goes out of the detector acceptance, the signal in the calorimeter is constant until the beam reaches the beam pipe. The distribution has been fitted with a Fermi-like function (Gaussian edged box) to evaluate the half-width and the Gaussian smearing at the edges. Taking into account that the calorimeter–magnet distance is $L = 1380$ mm, the half-width of the distribution is compatible with the nominal pipe radius, $r = 30$ mm: $(24 \pm 2) \times 10^{-3} \times 1380 = 33 \pm 3$ mm. The angular width of the Gaussian edge, i.e. when the beam hits the pipe wall, gives instead an indication of the beam spot size *at the line output*: $\sigma_x = (3.7 \pm 0.3) \times 10^{-3} \times 1380 = 5.0 \pm 0.4$ mm.

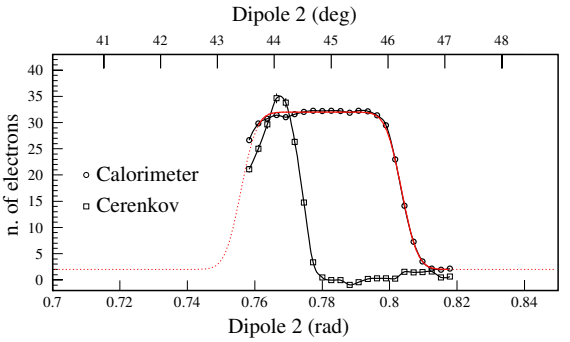

Fig. 25. Average number of electrons in the Cherenkov counter and in Calorimeter 2 as a function of the second dipole current, translated in bending angle in radians (bottom scale) and degrees (top scale), for $E_{sel} = 471$ MeV.

5. Operational experience

The very first commissioning of the BTF took place in February 2002 and after that all the measurements described in the previous sections and the first users data taking were performed in the period from October 29 to December 20, 2002.

During this phase, the DEAR experiment was running at the second interaction point of the DAΦNE Main Rings. This allowed to use the LINAC for BTF operation only between two injection cycles, in the so-called "parasitic mode". In the "dedicated mode", restricted to the maintenance/shutdown periods of the collider, the BTF runs 24 h per day.

During the 2002 DEAR runs, the typical bunch configuration in the Main Rings was $100 + 100$ colliding bunches. The typical injection cycle was

(1) the electrons were injected into the Accumulator and from there into the e^- Main Ring at 1 Hz repetition rate: 2–4 min required (100 bunches $\times 1$ s $\times$ no. of fillings);

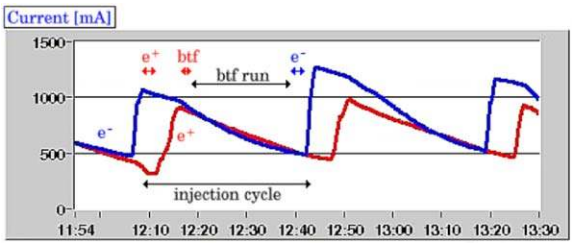

Fig. 26. Time chart of the electron and positron currents in the Main Rings showing a typical 'parasitic' BTF run: after the injection in the electron Main Ring the LINAC is switched for the positron injection (~3.5 min for switching); once the e^+ injection is completed the LINAC is switched to the BTF mode (~1.5 min). The BTF run lasts up to the next electron injection (3.5 min again needed to switch to e^-). During the DEAR operation the electron beam was injected every ≈40 min and the BTF duty cycle was about 50%.

(2) the LINAC and transferlines were switched to positron mode; 3.5 min were typically required (magnets ramping);
(3) positrons were injected into the Accumulator/e^+ ring at 1 Hz; 2–4 min were required;
(4) DEAR run started, and the injector was switched to the BTF mode with target and collimator slits inserted. The BTF magnets were cycled and ramped in 1–2 min;
(5) the BTF beam was delivered until 3.5 min before next DEAR injection; typically 20–25 min.

The described cycle required 40–45 min. Fig. 26 shows the time chart of the e^+/e^- currents in the Main Rings for a couple of injection cycles during the DEAR data taking. The different phases enumerated above are also indicated. In this condition the duty-cycle for the BTF operation was about 50%.

During the operation with the KLOE experiment, the injector operates in the "topping up" mode without interruption in the experiment data taking. A complete injection cycle in this mode of operation requires only 15–20 min leaving no real time for a parasite use of the BTF.

Another feature of the "parasitic mode" is that the LINAC energy cannot be easily changed during the reduced amount of time between two contiguous injections of DAΦNE.

6. Conclusions and future perspectives

The commissioning results, as well as the first user experience, have demonstrated that the DAΦNE Beam Test Facility can operate at a very high level of reliability. The BTF also showed a high versatility in operating with different configurations with energy included between 50 and 500 MeV and multiplicity from single to ≈1000 electrons.

In order to overcome the present limitations imposed by the KLOE operation, where the BTF cannot operate, and also to improve the duty cycle during the parasite mode of operation we are planning a BTF upgrade to be performed in January 2004 during the DAΦNE cryogenic system maintenance shutdown [14].

In the upgraded scheme, an improved separation between the LINAC to Accumulator transferline and the BTF channel will allow to operate the BTF in a mode where the only limitations will be due to the LINAC switching time and to the time spent for filling the Main Rings. A duty-cycle of order of 80% during the KLOE runs and around 90% for the FINUDA ones is expected.

More diagnostic systems, especially devoted to beam profiling and to high multiplicity measurements, are presently under development for improving the characterization and the quality of the BTF beams.

Acknowledgements

We want to warmly acknowledge M. Preger and F. Bossi for the revision of this work and the close and friendly collaboration of P. Privitera and of the AIRFLY group for the development of the Cherenkov detector.

We have also profited from the help and the suggestions of a number of LNF researchers: S. Bertolucci, G. Di Pirro, A. Esposito, S. Miscetti, P. Raimondi, A. Stella and M. Vescovi.

We deeply thank the technical staff of the Divisione Acceleratori for the operation of the facility and in particular for the tuning of the LINAC and for the set-up of the BTF hardware: G. Baldini, M. Belli, R. Clementi, O. Coiro, F. Galletti, O. Giacinti, E. Grossi, M. Martinelli, D. Pellegrini, R. Pieri, G. Piermarini, R. Zarlenga.

Finally we are grateful to the technicians of the Divisione Ricerca, in particular to M. Anelli, R. Rosellini, E. Turri, and M. Iannarelli, for their collaboration in the preparation of the experimental setup.

Work partially supported by TARI contract HPRI-CT-1999-00088.

References

[1] The DAΦNE project team, proposal for a ϕ-factory, LNF-90/031 1990;
S. Guiducci, et al., Status report on DAΦNE, in: Proceedings of PAC 2001, Chicago, USA, 2002.

[2] F. Sannibale, G. Vignola, DAΦNE Technical note LC-2, 1991, unpublished DAΦNE notes are available at http://www.lnf.infn.it/acceleratori/ A. Ghigo, F. Sannibale, Single electron operation mode in DAFNE BTF, in: Proceedings of EPAC 94, London, 1994, p. 2444.

[3] G. Di Pirro, et al., The evolution of the DAΦNE control system: a history of liberation from hardware, in: Proceedings of ICALEPCS 2001, San Jose, USA, 2002.

[4] O. Coiro, G. Galletti, DAΦNE Technical note CD-11, 2001, unpublished, DAΦNE notes are available at http://www.lnf.infn.it/acceleratori/.

[5] F. Sannibale, M. Vescovi, LINAC to accumulator area transferline and DAFNE-LINAC spectrometer, DAΦNE Technical note LC-3, 1992, unpublished, DAΦNE notes are available at http://www.lnf.infn.it/acceleratori/.

[6] A. Battisti, et al., Measurement and tuning of DAΦNE accumulator dipoles, DAΦNE Technical note MM-9, 1995, unpublished, DAΦNE notes are available at http://www.lnf.infn.it/acceleratori/; M. Preger, private communication.

[7] B. Rossi, High Energy Particles, Prentice-Hall, NY, USA, 1952.

[8] GEANT 3.21, CERN Program Library, Long Writeup W5013.

[9] D.C. Carey, et al., SLAC-R-530, 1998.

[10] A. Aloiso, et al., Nucl. Instr. and Meth. A 482 (2002) 363.

[11] A. Antonelli, et al., Nucl. Instr. and Meth. A 354 (1995) 352.

[12] G. Mazzitelli, et al., Nucl. Instr. and Meth. A 486 (2002) 568.

[13] P. Privitera, et al., AIRFLY Letter of Intent, INFN Gr. V, unpublished.

[14] G. Mazzitelli, et al., DAFNE beam test facility upgrade proposal, DAΦNE Technical note BTF-1, 2003, unpublished, DAΦNE notes are available at http://www.lnf.infn.it/acceleratori/.